Applied Surface Science 448 (2018) 154–162

Contents lists available at ScienceDirect

Applied Surface Science

journal homepage: www.elsevier.com/locate/apsusc

Full Length Article

XPS study of ion irradiated and unirradiated CeO_2 bulk and thin film samples

Konstantin I. Maslakov [a], Yury A. Teterin [a,b], Aleksej J. Popel [c,*], Anton Yu. Teterin [b], Kirill E. Ivanov [b], Stepan N. Kalmykov [a,b], Vladimir G. Petrov [a], Peter K. Petrov [d], Ian Farnan [c]

[a] Chemistry Department, Lomonosov Moscow State University, Moscow 119991, Russia
[b] NRC "Kurchatov Institute", Moscow 123182, Russia
[c] Department of Earth Sciences, University of Cambridge, Downing Street, Cambridge CB2 3EQ, United Kingdom
[d] Department of Materials and London Centre for Nanotechnology, Imperial College London, London SW7 2AZ, United Kingdom

ARTICLE INFO

Article history:
Received 5 March 2018
Revised 6 April 2018
Accepted 9 April 2018
Available online 10 April 2018

Keywords:
XPS
CeO_2
Electronic structure
Ionic composition
Thin film
Radiation damage

ABSTRACT

This work considers the effect of fission-energy ion irradiation on the electronic structure at the surface of bulk and thin film samples of CeO_2 as a simulant for UO_2 nuclear fuel. For this purpose, thin films of CeO_2 grown on Si substrates and bulk CeO_2 samples were irradiated by Xe ions (92 MeV, 4.8×10^{15} ions/cm^2) to simulate the fission damage that occurs within nuclear fuels. The irradiated and unirradiated samples were characterized by X-ray photoelectron spectroscopy. A technique of the quantitative evaluation of cerium ionic composition on the surface of the samples has been successfully applied to the obtained XPS spectra. This technique is based on the intensity of only one of the reliably identifiable high-energy peak at 916.6 eV in the Ce 3d XPS spectra. The as-produced samples were found to contain mostly the Ce^{4+} ions with a small fraction of Ce^{3+} ions formed on the surface in the air or under X-rays. The core-electron XPS structure of CeO_2 was associated with the complex final state with vacancies (holes) resulting from the photoemission of an inner electron. The Xe ion irradiation was found to increase the Ce^{3+} content in the samples of CeO_2, with the thin films being more sensitive than the bulks samples.

1. Introduction

Cerium dioxide, CeO_2, is a fluorite structure ceramic widely used as an inactive structural surrogate to UO_2 and PuO_2 to avoid difficulties associated when working with radioactive materials [1,2]. This material is suggested to be used as an inert matrix for perspective nuclear fuels and highly radioactive waste disposal [1,3]. Irradiation studies, where CeO_2 is exposed to ions with different mass and energy, are extensively taking place in the recent time [1,2,4–12]. The attempt of these studies is to replicate the effect of radiation damage by fission fragments that is taking place in UO_2 based fuels [13–18]. X-ray photoelectron spectroscopy (XPS) proved to be an effective tool for determination of the cerium ionic composition (Ce^{3+} and Ce^{4+}).

Unfortunately, the available literature does not reveal any information on dissolution mechanism of CeO_2 in water, but it is widely accepted that CeO_2 dissolves via reduction of Ce^{4+} to Ce^{3+} under air atmosphere [19]. It is also known that fission-energy ion irradiations of CeO_2 cause a partial reduction of Ce^{4+} to Ce^{3+} [7,20,21], which enhances its dissolution [19]. As a result, there is a practical need in a technique for quantitative evaluation of cerium ionic composition on the surface of CeO_2 samples to inform on their aqueous durability.

XPS determination of the cerium oxidation state in compounds faces difficulties due to the complex structure in the valence- and core-electron spectra [22–31]. Thus, the Ce 3d XPS spectra of the Ce^{3+} ions beside the primary peaks show sometimes the satellites with a higher intensity compared to the primary peaks [27,28,32–36]. The Ce 3d XPS spectra of CeO_2 show even more complicated structure [7,23,27,31,33–38] as compared to the spectra structure of Ln_2O_3 [22,23]. The majority of the available literature suggests that CeO_2 contains a mixture of Ce^{3+} and Ce^{4+} ions (mixed valence) [24–26,39,40]. However, the authors of Ref. [41] showed on the basis of the calculations that CeO_2 contains only Ce^{4+} ions, and the Ce 3d structure appears due to the complex final state containing the ground state Ce $3d^94f^0$ and two exited final states $3d^94f^1OVMO^{-1}$ and $3d^95p^5np^1$. These results agree with the experimental data of Ref. [42]. An unusual final state Ce $3d^95p^5np^1$ can be associated with the screened vacancy in the inner valence molecular orbitals (IVMO) [23,43]. The formation of such a vacancy agrees with the unusually high (16 eV) binding

* Corresponding author.
E-mail address: apopel@cantab.net (A.J. Popel).

https://doi.org/10.1016/j.apsusc.2018.04.077
0169-4332/

energy (BE) shift of the peaks associated with the final state Ce $3d^95p^5np^1$ relative to the peaks associated with the ground final state Ce $3d^94f^0$.

The complex XPS structure parameters can be used for qualitative identification of physicochemical properties in various cerium compounds [23] and the main attention is focused on the Ce 3d structure. Thus, on the basis of many Ce 3d XPS parameters, the authors of Ref. [44] suggest a technique of quantitative determination of the cerium ionic composition (Ce^{3+} and Ce^{4+}) in different compounds. The authors of Refs. [7] and [20] determined the Ce^{3+} concentration after irradiation of CeO_2 with 200 MeV Xe ions by direct subtraction of the Ce 3d spectrum of the Ce^{4+} ions of a standard sample from the Ce 3d spectrum of the irradiated sample. Similar techniques were used in Refs. [32,33,45–47].

This work considers the explicit effect of radiation damage by fission-energy ions on non-stoichiometry in CeO_2 as an inactive analogue to the UO_2 matrix of nuclear fuel and outlines a methodology developed for determining the degree of non-stoichiometry in CeO_{2-x}. For this purpose, thin films of CeO_2 on Si substrates and bulk CeO_2 samples were irradiated with $^{129}Xe^{23+}$ ions of 92 MeV to a fluence of 4.8×10^{15} ions/cm^2 to simulate the damage produced by fission fragments in nuclear fuel. The irradiated and unirradiated samples were analyzed using a quantitative analysis technique of the XPS spectra described in Ref. [35] and the obtained results were compared.

The XPS spectra in the present work were taken from the surface of single-crystal CeO_2 film in the BE range of 0–1250 eV in order to illustrate the complex structure formation in the Ce $3p_{3/2}$-, 3d-, 4s-, 4p-, 4d-, 5s-spectra (and the absence of the complex structure in the Ce 5p spectrum, where the quasi-core hole appears). Each of the measured spectra allowed a quantitative ionic composition to be evaluated on the basis of the technique considered in Ref. [35]. For the bulk samples the XPS spectra were measured for certain shells. A similar work has been done using UO_2 thin films in Ref. [48].

2. Experimental section

2.1. Sample production and irradiation

The CeO_2 thin films were grown by pulsed laser deposition (PLD) on three (001) oriented p-doped Si substrates and characterized as described in detail in Ref. [19]. The thin films of CeO_2 were nominally of the same thickness (250 nm), as they were deposited by the same number of laser pulses, the three samples produced had different colors. This is an indication that the thin films may have had different thicknesses [49]. X-ray diffraction (XRD) analysis suggested that the CeO_2 films of samples AP1 and AP3 can be described as single crystals in (1 1 1) crystallographic orientation and the CeO_2 film of sample AP2 is preferentially oriented in (1 1 1) with (0 0 1) domains also present. Sample AP1 was left as a benchmark for comparison and samples AP2 and AP3 were irradiated with Xe ions. The bulk samples of CeO_2 were obtained from Sigma-Aldrich in the form of fused pieces 3–6 mm in size and 99.9% purity on trace metal basis, as claimed by the supplier. Table 1 summarizes the produced and irradiated samples.

Table 1
Summary of the produced and irradiated CeO_2 samples.

Sample name	Sample description
AP1	Unirradiated thin film sample
AP2g	$^{129}Xe^{23+}$ irradiated thin film sample
AP3g	$^{129}Xe^{23+}$ irradiated thin film sample
AP4	Unirradiated bulk sample
AP4g	$^{129}Xe^{23+}$ irradiated bulk sample
AP5	Unirradiated bulk sample
AP5g	$^{129}Xe^{23+}$ irradiated bulk sample

These samples were studied earlier by XRD and scanning electron microscopy (SEM) and dissolution experiments were also performed to assess the effect of induced radiation damage on aqueous durability of the CeO_2 matrix in Ref. [19].

To simulate the damage produced by fission fragments in nuclear fuel, the samples were irradiated with 92 MeV energy $^{129}Xe^{23+}$ ions to a fluence of 4.8×10^{15} ions/cm^2 on the IRRSUD beamline at the GANIL accelerator, Caen, France, with a detailed description given in Ref. [19]. The SRIM code [50] indicated that the projected ion range in CeO_2 is ~7.5 μm and Xe ions completely penetrate the CeO_2 thin films (250 nm max) and stop in the substrate at a depth of ~13.5 μm beneath the sample's surface. The electronic stopping regime dominates the dissipation of ion energy throughout the entire film [19].

2.2. X-ray photoelectron measurements

X-ray photoelectron spectra of the CeO_{2-x} samples were recorded on a Kratos Axis Ultra DLD spectrometer using monochromatic Al-Kα radiation ($h\nu$ = 1486.7 eV) at 150 W X-ray gun power under 1.3×10^{-7} Pa at room temperature (Fig. 1). The analyzed area was an ellipse with 300 and 700 μm minor and major axes, respectively. Binding energy scale of the spectrometer was preliminarily calibrated by the position of the peaks of Au $4f_{7/2}$ (83.96 eV) and Cu $2p_{3/2}$ (932.62 eV) core levels for pure gold and copper metals. The spectra were acquired in the constant analyzer energy mode using the pass energy of 20 eV and a step size of 0.05 eV.

All the spectra were recorded as a sequence of one scan acquisition for each spectrum starting with the higher BE ones. The sequence was cycled until a certain spectrum measurement had reached a required number of scans, then the measurement of this spectrum would stop. The number of scans for each spectral peak was different depending on the intensity of this peak in the survey spectrum. This provided reliable spectral data and a correct BE calibration relative to the E_b(C 1s), peak width calibration relative to the Γ(C 1s), as well as the intensity calibration relative to the standard peak (e.g., Ce 3d).

The Kratos charge neutraliser system was used and BEs were measured relative to the BE of the C 1s electrons from hydrocarbons adsorbed on the sample surface that was accepted to be equal to 285.0 eV on the gold plate E_b(Au $4f_{7/2}$) = 84.0 eV and E_b(C 1s) =

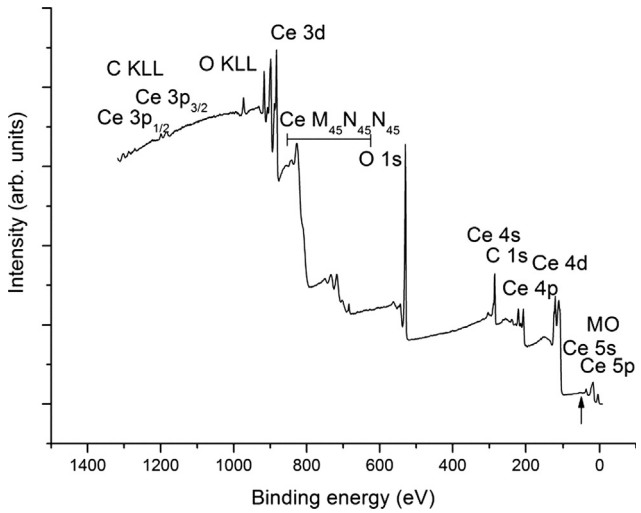

Fig. 1. XPS survey-scan of CeO_2 film (sample AP1).

284.1 eV. These values have to be taken into account for comparison of the present data with the data of other authors. The equipment resolution measured as the full width at half maximum (FWHM) of the Au $4f_{7/2}$ peak was less than 0.65 eV. The FWHMs are given relatively to that of the C 1s XPS peak from hydrocarbon on the sample surface being 1.3 eV [51]. The error in the determination of the BE and the peak width did not exceed ±0.05 eV, and the error of the relative peak intensity – ±5%. The inelastically scattered electron-related background was subtracted by the Shirley method [52].

A quantitative elemental analysis was performed for the surface of the studied samples. It was based on the fact that the spectral intensity is proportional to the number of certain atoms in the sample. The following ratio was used: $n_i/n_j = (S_i/S_j)(k_j/k_i)$, where n_i/n_j is the relative concentration of the atoms, S_i/S_j is the relative core–shell spectral intensity, k_j/k_i is the relative experimental sensitivity coefficient. The following coefficients relative to the C 1s were used: 1.00 (C 1s); 2.81 (O 1s); 0.119 (O 2s); 31.68 (Ce 3d); 0.68 (Ce 4s); 3.83 (Ce 4p); 8.860 (Ce 4d).

2.3. Determination of the ionic composition in CeO_{2-x} oxides

On the basis of the Ce 3d XPS structure and the technique described in Ref. [35] cerium ionic composition (Ce^{3+} and Ce^{4+}) of the studied samples was evaluated. The point of this technique was the following. The Ce 3d XPS of the Ce^{4+} ion consists of six peaks (1–6) corresponding to different final states after the Ce 3d electron photoemission (for line identification of this structure see Section 3, Fig. 2a). The Ce 3d XPS spectrum of a Ce^{3+} ion consists of four peaks located near the peaks (1, 4) and (2, 5) of the Ce^{4+} XPS spectrum (Fig. 2b, Ref. [35]). In the case of Ce^{3+} and Ce^{4+} mixture, the XPS spectrum is complicated. The feature I_0 (6) at 916.4–916.6 eV remains well pronounced (Fig. 2b). Shake-up satellites (3, 6) (Fig. 2a) are the Ce 3d spin-orbit doublet with ΔE_{sl}(Ce 3d) = 18.3 eV and shifted by 16.0 eV to the higher BE side relative to the spin-orbit doublet (1, 4) of the ground state. This doublet allows the most precise determination of the Ce 3d spin-orbit splitting. Since the feature (3) is the low-BE component of the spin-orbit doublet (3, 6), its intensity is (3/2) of I_0. Features (1, 2, 3) characterize only the Ce $3d_{5/2}$ spectrum. For the standard CeO_2 sample the intensity ratio (1, 2) to (3) is $a_0 = I_s/[(3/2)I_{0s}]$, where I_s is the intensity of features (1, 2), I_{0s} – is the intensity of feature (6) of standard Ce^{4+} spectrum, and a_0 is a calibration coefficient. Since the Ce $3d_{5/2}$ XPS features of the Ce^{3+} ions for the Ce^{3+} and Ce^{4+} mixture lies in the BE range of the features (1, 2) of Ce^{4+} XPS spectrum, using the calibration coefficient a_0 one can find the Ce^{3+} contribution to the XPS intensity.

If for the XPS spectrum of the Ce^{3+} and Ce^{4+} mixture I_0 is the intensity of feature (6); $(3/2)I_0$ is the intensity of feature (3); a_0 is the calibration coefficient; I is the intensity of features (1–2), including the Ce $3d_{5/2}$ intensity from the Ce^{3+} ions, then $a_0(3/2)I_0$ is the contribution of intensity of the Ce^{4+} ions to I; and $[I - a_0(3/2)I_0]$ is the contribution of the Ce^{3+} in the intensity I. Since the total Ce $3d_{5/2}$ intensity of the peaks (1–2–3) from the Ce^{3+} and Ce^{4+} ions is $[I + (3I_0/2)]$, the fraction $v_1(Ce^{3+})$ of the Ce^{3+} ions can be found as the ratio $[I - a_0(3/2)I_0)]$ to $[I + (3/2)I_0]$:

$$v_1(Ce^{3+}) = [1 - a_0(3/2)(I_0/I)]/[1 + (3/2)(I_0/I)] \quad (1)$$

and the fraction $v_2(Ce^{4+})$

$$v_2(Ce^{4+}) = 1 - v_1(Ce^{3+}). \quad (2)$$

As shown in the current work (Section 3), the similar expressions can be drawn using the Ce $3p_{3/2}$, 4s, 4p, 4d, 5s XPS structure parameters as well (Figs. 3–7). The results of Eqs. (1) and (2) for the surfaces of K-Ce-Ti ceramics are in a good agreement with the XRD and SEM-EDS data characterizing the bulk of the samples in Ref. [35].

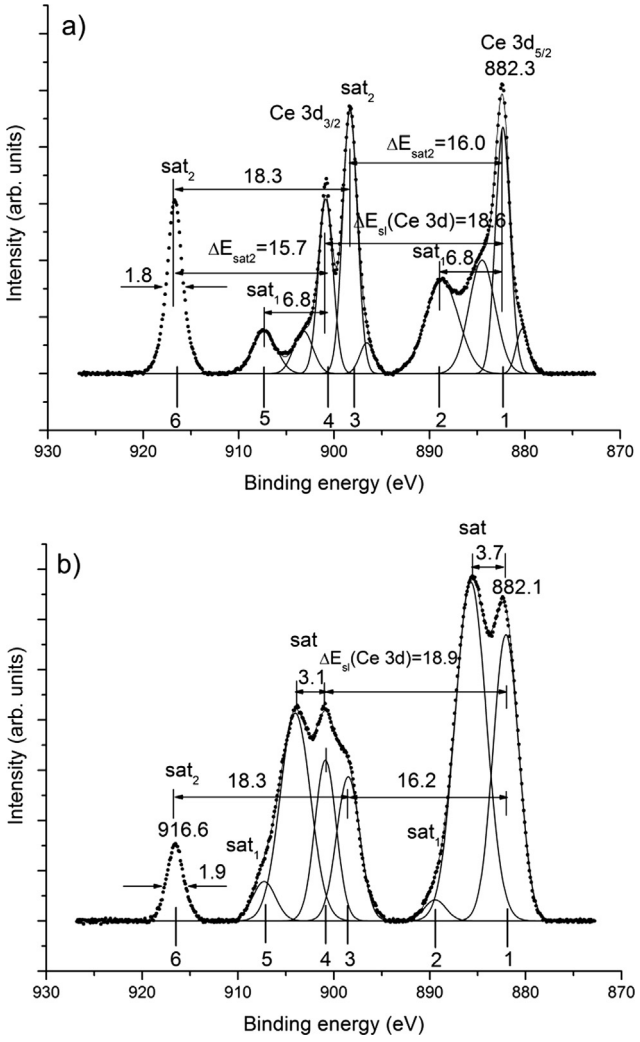

Fig. 2. Ce 3d XPS narrow-scans of the CeO_2 films: (a) unirradiated CeO_2 surface (sample AP1); (b) $^{129}Xe^{23+}$ irradiated surface (sample AP3g). Numbers under the spectra denote the structures associated with the ground Ce $3d^94f^0$ (1, 4) and excited Ce $3d^94f^1VMO^{-1}$ (2, 5) and Ce $3d^95p^54f^0np$ (3, 6) final states.

3. Results and discussion

The obtained results were discussed in the approximation that the standard CeO_2 sample contains only Ce^{4+} ions [42]. The survey XPS scans of all the studied cerium dioxide samples (Table 1) except for AP3g showed the XPS and Auger features only from cerium, oxygen and carbon (Fig. 1). The survey scan of AP3g showed extra peaks from Si 2s and 2p due to the film fragmentation under the Xe irradiation, which was seen in SEM (see Fig. 4 in Ref. [19]). Silicon was not observed in the XPS scans of AP1 and AP2g since their thickness (~250 nm) exceeded the photoelectron escape depth (~5 nm). The survey XPS scans are in satisfactory agreement with the data in Refs. [53] and [54].

3.1. The structure of XPS spectra of valence electrons

The valence (from 0 to ~50 eV BE) XPS structure of sample AP1 (Fig. 3a) differs slightly from the corresponding structure of CeO_2

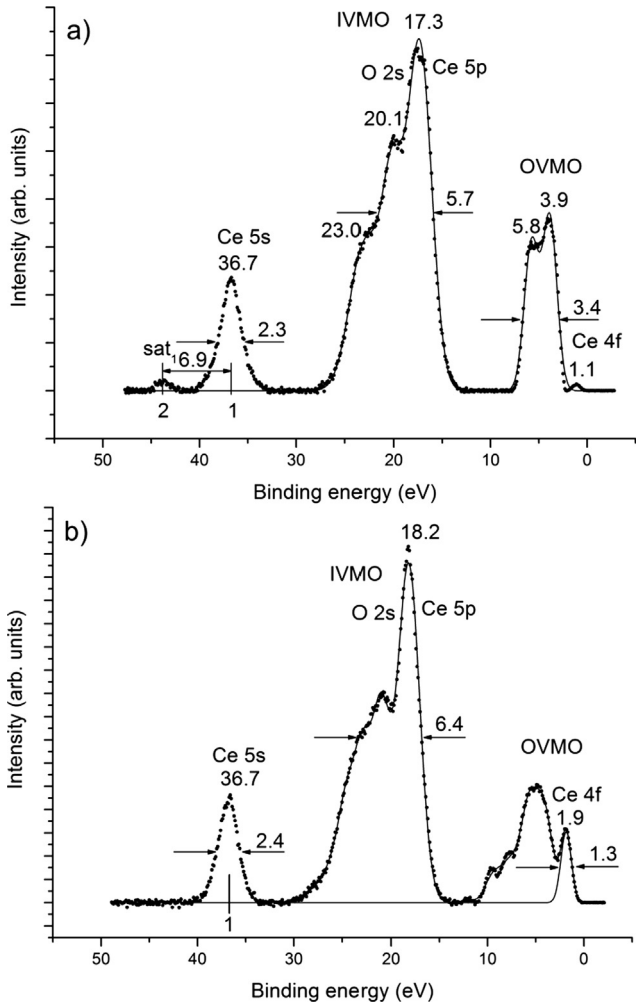

Fig. 3. Valence XPS narrow-scans of the CeO_2 thin film samples: (a) unirradiated CeO_2 surface (sample AP1); (b) $^{129}Xe^{23+}$ irradiated surface (sample AP3g). Numbers (1, 2) denote the final states (see Fig. 2). Peak (3) at 51.7 eV is not shown.

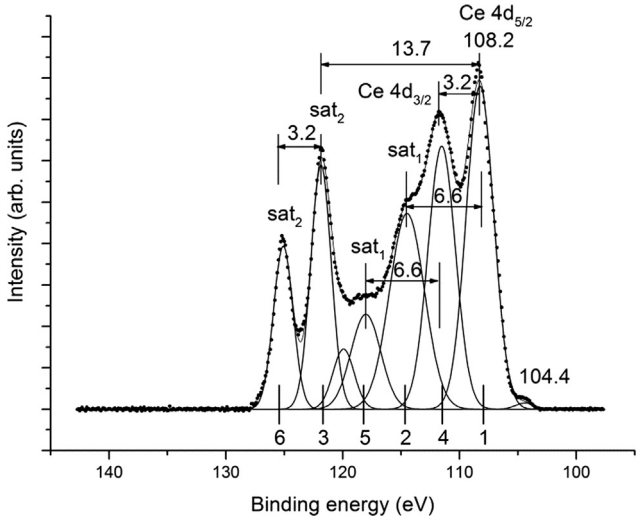

Fig. 4. Ce 4d XPS narrow-scan of unirradiated CeO_2 surface (sample AP1). Numbers (1–6) denote the final states (see Fig. 2).

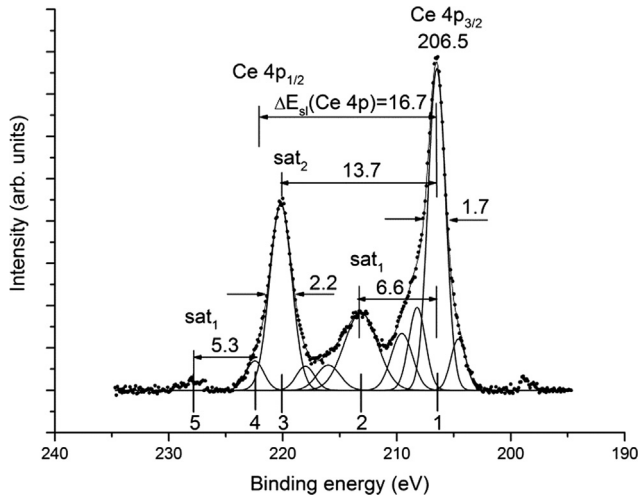

Fig. 5. Ce 4p XPS narrow-scan of unirradiated CeO_2 surface (sample AP1). Numbers (1–5) denote the final states (see Fig. 2). Peak (6) at 237.1 eV is not shown.

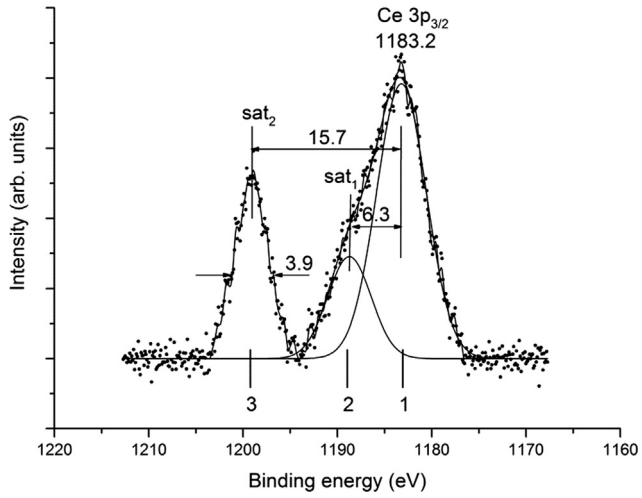

Fig. 6. Ce $3p_{3/2}$ XPS narrow-scan of unirradiated CeO_2 surface (sample AP1). Numbers (1, 2, 3) denote the final states (see Fig. 2). Peaks (4, 5, 6) at 1270.2, 1276.5 and 1285.9 eV are not shown.

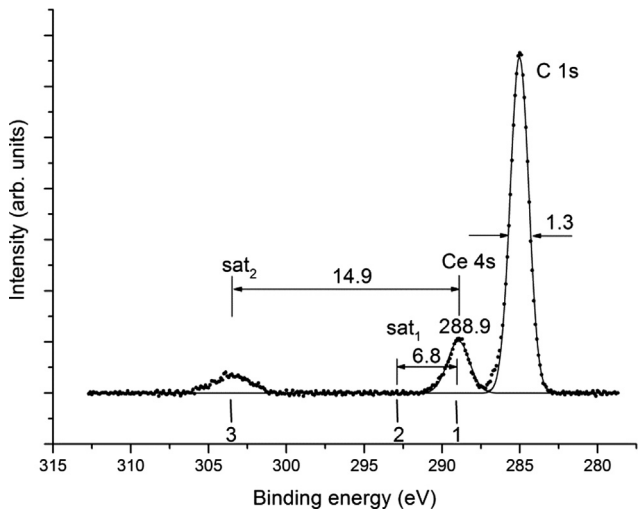

Fig. 7. XPS narrow-scans of Ce 4s and C 1s of unirradiated CeO_2 surface (sample AP1). Numbers (1, 2, 3) denote the final states (see Fig. 2).

samples in Refs. [23] and [42]. Beside the structures associated with the outer (OVMO) and inner (IVMO) valence molecular orbitals, this spectrum shows a low-intensity peak at 1.1 eV associated with the unbound Ce 4f electrons (Table 2) of the Ce^{3+} ions formed on the surface in the air and/or under the X-ray beam in the spectrometer chamber [34,44,55,56]. The Ce 4f peak must be absent for compounds containing only Ce^{4+} ions, while for compounds containing Ce^{3+} ions this peak must have a high intensity being an important characteristic of the Ce^{3+} ions [23,42]. This was confirmed by the absence of the Ce 4f peak in the photoelectron spectrum (350 eV excitation) of a single-crystalline CeO_2 (1 1 0) film on a $SrTiO_3$ (2 1 1) single crystal substrate in Ref. [57], in the spectrum of valence electrons of a CeO_2 film on a Ge substrate [58] and in the valence electron resonant emission spectrum (Ce 4f → Ce $4\underline{d}^1$) of cerium dioxide samples in Ref. [57]. The Ce 4f peak is also absent in the spectrum of a fresh CeO_2 powder pressed in an indium holder measured under the AlK_α X-ray beam exposure for ~20 min in Ref. [42]. The resonant emission spectrum of Ce_2O_3, as expected, shows the intense Ce 4f peak at 1.9 eV [57]. The authors of Ref. [57] showed that Ce^{4+} ions on the surface of CeO_2 powder samples reduce to Ce^{3+} ions under the X-ray irradiation faster than on the surface of sintered samples. Such partial Ce^{4+} to Ce^{3+} reduction also takes place during heating of a CeO_2 sample up to 900 °C in a sample chamber of the XPS spectrometer [59,60]. The examined samples can also be heated under the AlK_α X-ray irradiation. Therefore, the low-intensity peak at 1.1 eV in the XPS spectrum of sample AP1 (Fig. 3a) should be attributed to Ce^{3+} ions formed under the excitation X-ray beam. Since the Ce^{3+} ion content in sample AP1 is just several percent, the main XPS structure typical for Ce^{4+} ions remains.

The intensity of the peak associated with the unbound Ce 4f electrons $I_{Ce4f} = I(Ce\ 4f)/I(Ce\ 5s)$ relative to the intensity of the Ce 5s peak taking into account the satellite intensities and with the photoionization cross-sections in mind [61,62] allowed a quantitative evaluation of the number of the Ce 4f electrons per one cerium atom n_{Ce4f} for the studied samples (Table 3) with the accuracy of ±5%, since the Ce 4f intensity is very low compared to the Ce 5s intensity. These data show that for sample AP1 $n_{Ce4f} = 0.03$ and this sample contains 3% of Ce^{3+} ions. An XPS spectrum of sample AP1 contains mostly the Ce^{4+}-related structure with weak Ce^{3+}-related features.

The OVMO spectrum of sample AP1 show two peaks at 3.9 and 5.8 eV and is 3.4 eV wide (Γ(OVMO) = 3.4 eV) (Fig. 3a, Table 2). On the basis of the valence resonant emission spectral structure of CeO_2 [57] and non-relativistic calculation results for the CeO_8^{12-} cluster [43] the peak at 3.9 eV can be attributed to the Ce 4f – O 2p states, and the peak at 5.8 eV – to the Ce 5d – O 2p states. The IVMO XPS structure contains three peaks at 17.3, 20.1 and 23.0 eV (Fig. 3a), which agrees qualitatively with the calculation results in Ref. [43].

3.2. The structure of XPS spectra of inner electrons

The Ce 5s XPS structure contains the primary line at E_b(Ce 5s) = 36.7 eV with a width Γ(Ce 5s) = 2.3 eV and at 6.9 eV away from the primary peak exhibits a 4% intensity satellite associated with the charge transfer effect during the photoemission, and a ~50% intensity shake-up satellite 15 eV away from the primary peak, which is not shown in Fig. 3a but indicated in the survey spectrum (Fig. 1) with an arrow. It should be noted, that such satellites are absent

Table 2
Electron binding energies E_b[a] (eV), FWHM Γ[b] (eV), satellite positions E_{sat}[c] (eV) of the unirradiated (AP1, AP4, AP5) and $^{129}Xe^{23+}$ irradiated (AP2g, AP3g, AP4g, AP5g) cerium dioxide films and bulk samples.

Sample	Ce 4f	OVMO	Ce $5p_{3/2}$	Ce 5s	Ce $4d_{5/2}$	Ce $4p_{3/2}$	Ce 4s	Ce $3d_{5/2}$	O 1s
AP1[d]	1.1	3.9 (1.6) 5.8 (1.7)	17.3 – –	36.7 (2.3) 6.9 sat_1 15 sat_2	108.2 (2.7) 6.6 sat_1 13.7 sat_2	206.5 (1.8) 6.6 sat_1 13.7 sat_2	288.9 (1.6) 6.8 sat_1 14.9 sat_2	882.3 (1.5) 6.8 sat_1 16.0 sat_2	529.4 (1.0) 531.7 (2.0)
AP2g	1.1	4.0 (1.6) 5.9 (1.9)	17.6	36.9 (2.8) 6.8 sat_1			288.9 (1.9)	882.5 6.7 sat_1 15.9 sat_2	529.6 (1.1) 531.3 (1.8)
AP3g	1.9 (1.3)	4.1 5.7 7.6 9.4	18.2	36.7 (2.8) –			288.8 (2.1)	882.1 3.7 sat 6.8 sat_1 16.2 sat_2	530.2 (1.7) 531.8 (1.9)
AP4	1.2	3.9 5.7	17.7	36.7 (2.4) 6.7 sat_1			288.8 (1.5)	882.1 6.5 sat_1 16.0 sat_2	529.4 (1.1) 531.4 (1.9)
AP4g	1.3	4.1 5.3	18.0	36.8 (2.7) 6.8 sat_1			289.0 (1.9)	882.1 6.8 sat_1 15.9 sat_2	529.4 (1.2) 532.2 (1.4)
AP5	1.2	3.8 5.7	17.2	36.8 (2.5) 6.7 sat_1			289.0 (1.5)	882.1 6.2 sat_1 16.0 sat_2	529.4 (1.2) 531.3 (2.2)
AP5g	1.3	3.7 5.7	17.4	36.8 (2.9) 6.8 sat_1			288.9 (2.0)	882.0 6.1 sat_1 15.8 sat_2	529.5 (1.3) 531.7 (2.1)
CeO_2[e]		5.0	18.0	36.8	108.5 13.2 sat_2	207.1 13.2 sat_2	288.8 13.4 sat_2	882.3 6.5 sat_1 15.7 sat_2	529.5
$CeNbO_4$[e]	1.4	5.8	17.8		108.5		288.8	(881.8) 4.0 sat_1	530.0

[a] BEs are given relative to the E_b(C 1s) = 285.0 eV.
[b] FWHMs Γ(eV) are given in the parenthesis.
[c] Satellites s_1 are associated with the charge transfer effect, s_2 – with the shake-up process.
[d] Ce $3p_{3/2}$ spectrum consists of two peaks at 1183.2(7.4) and 1198.9(3.9) eV.
[e] BEs are given relative to the E_b(C 1s) = 285.0 eV for powders of CeO_2 and $CeNbO_4$ [42].

Table 3
Ionic compositions[a] Ce^{4+} and Ce^{3+} (%), oxygen coefficient[b] x in CeO_x and the number[c] of the Ce 4f electrons per one Ce atom n_{Ce4f} on the surface of the unirradiated and $^{129}Xe^{23+}$ irradiated samples.

Sample	Ce^{4+}	Ce^{3+}	x	n_{Ce4f}
AP1	97	3	2.0	0.03
AP2g	87	13	1.9	0.08
AP3g	29	71	1.7	0.77
AP4	96	4	2.7	0.03
AP4g	92	8	2.6	0.04
AP5	98	2	2.5	0.03
AP5g	93	7	2.3	0.04

[a] Ionic composition Ce^{4+} and Ce^{3+} (%), found from Eqs. (1) and (2).
[b] Oxygen coefficient x in CeO_x found using the primary O 1s intensity.
[c] Evaluation of the number n_{Ce4f} of the Ce 4f electrons per one Ce atom was done on the basis of the Ce 4f and Ce 5s XPS intensities taking into account the satellites and with photoionization cross-section in mind [61,62].

in the Ce 5p spectrum. On the one hand, the absence of intense satellites in the Ce 5p spectrum agrees with the fact that the Ce 5p electrons are not atomic and participate in the chemical bond formation. On the other hand, this experimentally corroborates that the Ce 5p electrons participate in the shake-up process responsible for the intense satellites at the higher BE side from the primary peaks (sat_2) in the core-electron XPS spectra of CeO_2 (Figs. 2, 4–6 in Refs. [36;42]).

The Ce 3d XPS structure of sample AP1 instead of the expected spin–orbit split (ΔE_{sl}(Ce 3d) = 18.6 eV) of two peaks exhibits a complex structure due to a complex final state after the Ce 3d electron photoemission (Fig. 2a, Table 2, Refs., [37;42]). One can separate 6 principal features in this structure (1–6) (Fig. 2a). The final state consists of three separate final states with holes: Ce $3d^94f^0$ – ground final state (1, 4) results in the spin-doublet (ΔE_{sl}(Ce 3d) = 18.6 eV) in the spectrum; Ce $3d^94f^1VMO^{-1}$ – charge transfer related satellites sat_1 (2, 5) with ΔE_{sat1}(Ce 3d) = 6.8 eV; Ce $3d^95p^54f^0np^1$ – shake-up satellites sat_2 (3, 6) with ΔE_{sat2}(Ce 3d) = 16.0 (15.7) eV (Refs. [41;42], Fig. 2a). The state Ce $3d^95p^54f^0np^1$ unlike the other states contain an extra quasi-core hole Ce $\underline{5p}^1$ resulting in a strong shift of the doublet (3, 6) toward the higher BE side relative to the doublet (1, 4), which is associated with the ground final state. The total intensity of all the complex structure for the standard stoichiometric CeO_2 corresponds to Ce 3d electrons of the Ce^{4+} ions only [35,42,63]. In Ref. [41] it is mentioned that the Ce $3d^94f^1VMO^{-1}$ state involves a 4f-electron. This results in multiplet splitting of the duplet. In other words, it is possible to say that the duplet lines of the Ce $3d^94f^0$ (1, 4) and Ce $3d^95p^54f^0np^1$ (3, 6) states must be narrow and the duplet lines of the Ce $3d^94f^1VMO^{-1}$ (2, 5) state will have a complex shape (see Fig. 2a). This shape is difficult for accounting during decomposition of the spectrum into components.

The complex structure in the Ce 4d XPS of sample AP1 (Fig. 4) also consists of 6 features and, as in the case of the Ce 3d XPS structure corresponds to the complex final state of cerium ions [42]: Ce $4d^94f^0$ – ground final state (1, 4) resulting in the spin-doublet (ΔE_{sl}(Ce 4d) = 3.2 eV); Ce $4d^94f^1VMO^{-1}$ – charge transfer related satellites sat_1 (2, 5) with ΔE_{sat1}(Ce 4d) = 6.6 eV; and Ce $4d^95p^54f^0$-np^1 – shake-up satellites (3, 6) with ΔE_{sat2}(Ce 4d) = 13.7 eV (Fig. 4, Table 2). At 104.4 eV BE one can see a very weak feature corresponding to Ce^{3+} ions present [55], which agrees with the weak feature in the valence band of the Ce 4f XPS spectrum (Fig. 3a).

The Ce 4p XPS structure is even more complicated compared to the Ce 4d one due to the fact that the Ce 4p spectrum exhibits the dynamic effect related structure (like the Ba 4p and La 4p XPS structure in compounds considered in Refs. [64;65]) together with the structures related to the spin-orbit splitting and the satellites. The dynamic effect appears due to the extra two-hole final state Ce $4p^64d^85p^64f^0np^1$, which results in the smearing of the primary structure, especially the Ce $4p_{1/2}$ component (Fig. 5). Five unmarked extra peaks in Fig. 5 are attributed to the dynamic effect. Despite this, one can see six components (1–6) quantitatively characterizing the Ce^{4+} ion. Ce $4p^54f^0$ – is the ground final state (1, 4); Ce $4p^54f^1VMO^{-1}$ – charge transfer related satellites (2, 5) and Ce $4p^55p^54f^0np^1$ – shake-up satellites (3, 6). Feature (6) is observed at the higher BE side from the (3) at 17 eV is not shown in Fig. 5. The Ce $3p_{3/2}$ spectrum, as well as the Ce $4p_{3/2}$ one, exhibits three features (1–3) associated with the final states: Ce $3p^3_{3/2}4f^0$ (1); Ce $3p^3_{3/2}4f^1VMO^{-1}$ (2); and Ce $3p^3_{3/2}5p^54f^0np^1$ (3) (Fig. 6).

The spectrum of Ce 4s electrons is observed toward high energies of bonding from the C 1s peak of saturated hydrocarbons with the intensity I_{C1s} (C 1s/Ce 3d) = 1.44 is observed at 285.0 eV (Fig. 7). The Ce 4s spectrum, like the Ce 5s one (Fig. 3a), consists of three features (1–3), corresponding to the final states: Ce $4s^14f^0$ – ground final state (1); Ce $4s^14f^1VMO^{-1}$ – 4% intensity charge transfer related satellite (2); and Ce $4s^15p^54f^0np^1$ – 50% intensity shake-up satellite. The observed complex structure in the XPS spectrum of the film in sample AP1 corresponds mostly to that of bulk samples AP4, AP5 and CeO_2 samples in Refs. [37] and [42]. The final state with the extra weakly-screened quasi-core hole Ce $\underline{5p}^1$ can probably be explained by the Ce^{4+} ion close environment structure. Indeed, if CeO_2 ($CeO_8^{12-}(O_h)$) concentration decreases and Ce_2O_3 ($CeO_7^{11-}(C_{3v})$) concentration increases [43], the feature associated with the Ce $\underline{5p}^1$ hole in the XPS spectrum decreases (see, e.g., Fig. 3).

The O 1s XPS spectrum of sample AP1 consists of the primary sharp (Γ(O 1s) = 1.0 eV) peak at 529.4 eV and a widened (Γ(O 1s) = 2.0 eV) feature at 531.7 eV of 26% intensity associated with hydroxyl groups (Fig. 8a). With Eq. (3) [66] in mind:

$$R_{E-O}\ (\mathrm{nm}) = 2.27(E_b - 519.4)^{-1} \quad (3)$$

one can evaluate a distance between an element and oxygen for the Ce–O corresponding to E_b(O 1s) = 529.4 eV as $R_{Ce\text{-}O}$ = 0.227 nm, and that corresponding to E_b(O 1s) = 531.7 eV – as $R_{Ce\text{-}O}$ = 0.185 nm. The value $R_{Ce\text{-}O}$ = 0.227 nm with an accuracy of 3% agrees with the value of 0.2344 for a CeO_2 from the crystallographic data in Ref. [44]. The oxygen coefficient x = 2.0 (CeO_x) for sample AP1 found on the basis of the O 1s primary peak intensity and the Ce 3d intensity and the corresponding sensitivity coefficients (see Section 2) is in a qualitative agreement with the expected value of 2 for CeO_2 (Table 3). In the cases of bulk samples AP4 and AP5 the oxygen coefficients exceed significantly the expected value (Table 3). In this case this technique does not allow a correct determination of the oxygen coefficient, as it was shown for uranium oxides UO_x in Ref. [48]. This can be explained by the presence of an excess oxygen on the surface of the bulk samples whose BE is the same as that for oxygen in CeO_2, which results in an increase in the line intensity of the O 1s-electrons in CeO_2. In this paragraph we determined that an additional structure, in all spectra of the inner electrons (Ce $3p_{3/2}$, 3d, 4s, 4p, 4d, 5s), is related to the same mechanism of multielectron excitation to a large extent. This allows using characteristics of the structure of these spectra for determination of the cerium ionic composition in CeO_{2-x} oxides.

3.3. XPS spectra of the irradiated samples

The spectrum of irradiated sample AP2g exhibits certain changes compared to that of unirradiated sample AP1 (Table 2), which agrees with the data of Refs. [7] and [20]. For sample AP3g more significant changes were observed due to the presence of Ce^{3+} ions [7,20]. In the valence band XPS spectrum of sample AP3g significant growth of the Ce 4f peak at 1.9 eV was observed (Fig. 3b). This agrees with the photoelectron spectrum of Ce_2O_3, obtained by Ar^+ etching of the surface of CeO_2, which exhibits the Ce 4f peak at 2.0 eV [55]. For sample AP2g the oxygen

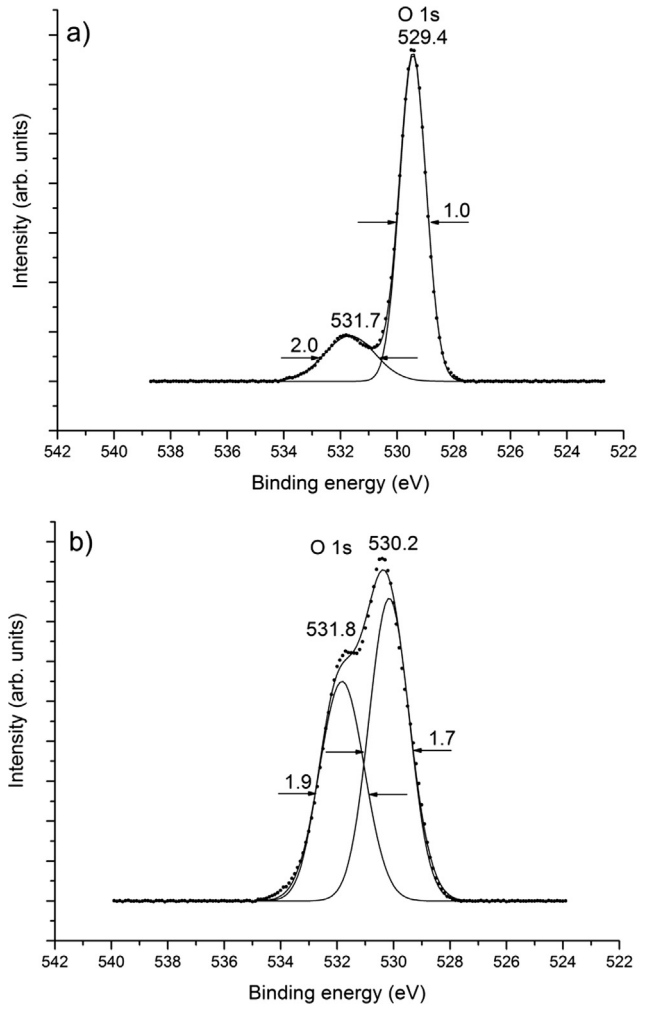

Fig. 8. O 1s XPS narrow-scans of CeO_2 surfaces: (a) unirradiated CeO_2 surface (sample AP1); (b) $^{129}Xe^{23+}$ irradiated surface (sample AP3g).

coefficient decreases to $x = 1.9$ due to the presence of Ce^{3+} ions (Table 3). An increase of the Ce 4f intensity in the XPS spectrum of sample AP3g relative to that of sample AP1 can be explained by an increase of the number of the $Ce^{3+}(4f^1)$ ions in sample AP3g, which also results in the Ce 5s and Ce 4s peaks widening due to the multiplet splitting (Table 2). However, this splitting is absent from the spectra of Ce^{4+} ions [67]. The vanishing of the satellite at 6.9 eV in the Ce 5s spectrum and complication of the IVMO spectrum can be explained by the destruction of the CeO_2 (CaF_2) structure [43].

The O 1s primary peak of sample AP3g appears 0.8 eV shifted and widened, an extra feature at 531.8 eV was attributed to oxygen from the Si substrate (Fig. 8b). This shift of the primary O 1s peak takes place due to the $CeO_2 \rightarrow Ce_2O_3$ transition [55,57]. Since E_b (O 1s) = 530.2 eV for sample AP3g (Table 2), with Eq. (3) in mind one can evaluate the mean interatomic distance $R_{Ce\text{-}O}$ in sample AP3g as 0.210 nm, which is significantly lower than $R_{Ce\text{-}O}$ = 0.227 nm in sample AP1. This indicates that the irradiation changes dramatically the CeO_2 structure and leads to a decrease of the $R_{Ce\text{-}O}$, which is significantly lower than the mean interatomic distance $R_{Ce\text{-}O}$ = 0.2505 nm (in the nearest environment of Ce in Ce_2O_3 there are 3 atoms of oxygen at a distance of 0.2339 nm for the first oxygen atom, 0.2434 nm for the second oxygen atom, and 0.2694 nm for the third oxygen atom) in Ce_2O_3 [40,68].

The core-level, in particular the Ce 3d, XPS spectrum of sample AP3g exhibits significant changes after irradiation (Fig. 2b). The Ce^{4+} charge transfer- (2, 5) and shake-up- (3, 6) related satellite intensities drops, while the intensity of satellites related to the Ce^{3+} charge transfer (ΔE_{sat} (Ce $3d_{5/2}$) = 3.7 eV) significantly grows. This indicates a decrease of the Ce^{4+} concentration and a growth of the Ce^{3+} concentration. Earlier, irradiation of thin film and bulk samples [7,20] of CeO_2 with 200 MeV Xe ions to a fluence of 10^{14} ions/cm^2 caused fewer changes in the Ce 3d spectral structure. Much fewer changes were also observed in the spectra of the bulk samples of cerium dioxide after irradiation (AP4g, AP5g) (Tables 2 and 3), which agrees with the data in Ref. [7].

3.4. Ionic composition of CeO_{2-x} oxides

The ionic composition (Ce^{4+} and Ce^{3+}) on the surface of the studied samples found by Eqs. (1) and (2) with the calibration coefficient a_0 = 2.0 within the measurement error of ±5% (Table 3) agrees with the data in Ref. [35]. The obtained results show that the surface of sample AP1 contains 97% of Ce^{4+} and 3% of Ce^{3+}, 2.0 atoms of oxygen for CeO_2 and 0.54 atoms of oxygen from hydroxyl groups. The 3% concentration of Ce^{3+} on the surface of sample AP1 (Table 3) agrees with the number of the Ce 4f electrons per one cerium atom being 0.03, which was found using the Ce 4f and Ce 5s intensities taking into account satellites and with photoionization cross-sections in mind [61,62]. For samples AP1, AP2g, and AP3g a correlation of the Ce^{3+} concentration with the oxygen coefficient x in CeO_x and the number of the Ce 4f electrons n_{Ce4f} was observed (Table 3).

In the $^{129}Xe^{23+}$ irradiated sample AP2g the Ce^{3+} concentration grew up to 13%, and the oxygen coefficient decreased to 1.9 compared to sample AP1 (Table 3). This agrees with the data in Ref. [20]. An increase of Ce^{3+} ions concentration to 71% was observed for irradiated sample AP3g. Such severe radiation damage can be explained by its low thickness. As noted, the CeO_2 samples were studied with the XRD, SEM and dissolution experiments in Ref. [19]. According to our evaluation with the dissolution and XPS data in mind, the film in sample AP2g is nominally about 20 times thicker than the film in sample AP3g. This agrees with the SEM data that show that the film in sample AP3g fragmented (the film in sample AP2g developed pores – see Fig. 3 in Ref. [19], the film in sample AP3g fragmented – see Fig. 4 in Ref. [19]). As a result, the XPS spectrum of sample AP3g exhibits intense Si 2s, 2p peaks, which were not observed in the XPS spectrum of samples AP1 (Fig. 1) and AP2g. Silicon-related features were not observed in the XPS of AP2g, since the spectra were taken from a continuous film region without pores (see Fig. 3 in Ref. [19]).

The valence and core-electron XPS spectrum of bulk samples AP4 and AP5 do not much differ from the corresponding spectra of sample AP1 (Fig. 3a, Table 2). The ion irradiation does not bring significant changes in their spectral structures (Table 3). This can be explained by the presence of excess oxygen on the surface that can oxidize the Ce^{3+} ions forming under the $^{129}Xe^{23+}$ irradiation. The spectral structure qualitatively show that the irradiated samples (AP4g and AP5g) contain more Ce^{3+} ions than the unirradiated ones (AP4 and AP5) (Table 3). This agrees with the data of other authors in Ref. [7]. In addition, the XPS measurements performed in Ref. [69] on unirradiated and Xe ion irradiated (under the same conditions) bulk samples of UO_2 indicated that the samples were subjected to significant surface oxidation, since the samples were cut and stored under an ambient air atmosphere, and surface oxidation has masked potential ion irradiation effects. Hence, no noticeable difference in the uranium ionic surface composition was observed between the irradiated and unirradiated samples.

4. Conclusions

High precision X-ray photoelectron spectra of the single crystal thin film (250 nm) CeO_2 on a silicon substrate (sample AP1) and

the polycrystalline CeO_2 fused pellets (AP4 and AP5) were taken in a wide binding energy range of 0–1250 eV.

It was shown that in the spectra of the inner Ce $3p_{3/2}$-, 4s-, 4p-, 4d-, 5s-electrons a complex structure forms which is linked mainly with the multielectron excitation. One of the final states of Ce^{4+} ion, formed by photoemission of an electron, contains a vacancy Ce $\underline{5p}^1$ in the Ce 5p orbital. This vacancy is virtually an inner vacancy and only weakly screened by the surrounding electrons. It results in intense lines in the spectrum which are unusually strongly shifted by ~14–16 eV toward higher bonding energies from the primary spectra lines.

The main cerium state in the film of sample AP1 was found to be $Ce^{4+}(4f^0)$. The Xe ion irradiation of the films (AP2g and AP3g) and bulk samples (AP4g and AP5g) was found to increase the concentration of the Ce^{3+} ($4f^1$) ions containing the unbound Ce 4f electrons manifested as a corresponding peak in the XPS spectra near the Fermi level. On the basis of the spectrum structure, in particular of the Ce 3d-electrons, the cerium ionic composition (Ce^{3+} and Ce^{4+}) of the samples was determined. The effect of the Xe ion irradiation on the ionic composition was more pronounced for the thin film rather than bulk samples.

Declarations of interest

None.

Acknowledgements

The work was supported by the RFBR grant № 17-03-00277a. The authors acknowledge support from Lomonosov Moscow State University Program of Development for providing access to the XPS facility. The irradiation experiment was performed at the Grand Accélérateur National d'Ions Lourds (GANIL) Caen, France, and supported by the French Network EMIR. The support in planning and execution of the experiment by the CIMAP-CIRIL staff and the GANIL technical staff, especially, I. Monnet, C. Grygiel, T. Madi and F. Durantel, is much appreciated. A.J. Popel acknowledges funding from the UK EPSRC (grant EP/I036400/1) and Radioactive Waste Management Ltd (formerly the Radioactive Waste Management Directorate of the UK Nuclear Decommissioning Authority, contract NPO004411A-EPS02), a maintenance grant from the Russian Foundation for Basic Research (projects 13-03-90916) and CSAR bursary.

References

[1] P.D. Edmondson, Y. Zhang, S. Moll, F. Namavar, W.J. Weber, Irradiation effects on microstructure change in nanocrystalline ceria – phase, lattice stress, grain size and boundaries, Acta Mater. 60 (2012) 5408–5416.
[2] M. Kinoshita, K. Yasunaga, T. Sonoda, A. Iwase, N. Ishikawa, M. Sataka, K. Yasuda, S. Matsumura, H.Y. Geng, T. Ichinomiya, Y. Chen, Y. Kaneta, M. Iwasawa, T. Ohnuma, Y. Nishiura, J. Nakamura, Hj. Matzke, Recovery and restructuring induced by fission energy ions in high burnup nuclear fuel, Nucl. Instr. Meth. Phys. Res. B 267 (2009) 960–963.
[3] B.E. Burakov, M.I. Ojovan, W.E. Lee, Crystalline materials for actinide immobilisation, in: W.E. Lee (Ed.), Materials for Engineering, vol. 1, Imperial College Press, London, 2011, pp. 58–59.
[4] T. Kishino, K. Shimizu, Y. Saitoh, N. Ishikawa, F. Hori, A. Iwase, Effects of high-energy heavy ion irradiation on the crystal structure in CeO_2 thin films, Nucl. Instr. Meth. Phys. Res. B 314 (2013) 191–194.
[5] K. Shimizu, S. Kosugi, Y. Tahara, K. Yasunaga, Y. Kaneta, N. Ishikawa, F. Hori, T. Matsui, A. Iwase, Change in magnetic properties induced by swift heavy ion irradiation in CeO_2, Nucl. Instr. Meth. Phys. Res. B 286 (2012) 291–294.
[6] Y. Tahara, B. Zhu, S. Kosugi, N. Ishikawa, Y. Okamoto, F. Hori, T. Matsui, A. Iwase, Study on effects of swift heavy ion irradiation on the crystal structure in CeO_2 doped with Gd_2O_3, Nucl. Instr. Meth. Phys. Res. B 269 (2011) 886–889.
[7] A. Iwase, H. Ohno, N. Ishikawa, Y. Baba, N. Hirao, T. Sonoda, M. Kinoshita, Study on the behavior of oxygen atoms in swift heavy ion irradiated CeO_2 by means of synchrotron radiation X-ray photoelectron spectroscopy, Nucl. Instr. Meth. Phys. Res. B 267 (2009) 969–972.
[8] N. Ishikawa, Y. Chimi, O. Michikami, Y. Ohta, K. Ohhara, M. Lang, R. Neumann, Study of structural change in CeO_2 irradiated with high-energy ions by means of X-ray diffraction measurement, Nucl. Instr. Meth. Phys. Res. B 266 (2008) 3033–3036.
[9] T. Sonoda, M. Kinoshita, Y. Chimi, N. Ishikawa, M. Sataka, A. Iwase, Electronic excitation effects in CeO_2 under irradiations with high-energy ions of typical fission products, Nucl. Instr. Meth. Phys. Res. B 250 (2006) 254–258.
[10] C.L. Tracy, M. Lang, J.M. Pray, F. Zhang, D. Popov, C. Park, C. Trautmann, M. Bender, D. Severin, V.A. Skuratov, R.C. Ewing, Redox response of actinide materials to highly ionizing radiation, Nat. Commun. 6 (2015) 6133.
[11] R.I. Palomares, J. Shamblin, C.L. Tracy, J. Neuefeind, R.C. Ewing, C. Trautmann, M. Lang, Defect accumulation in swift heavy ion-irradiated CeO_2 and ThO_2, J. Mater. Chem. A 5 (2017) 12193–12201.
[12] P.D. Edmondson, N.P. Young, C.M. Parish, S. Moll, F. Namavar, W.J. Weber, Y. Zhang, T. Mitchell, Ion-beam-induced chemical mixing at a nanocrystalline CeO_2-Si interface, J. Am. Ceram. Soc. 96 (2013) 1666–1672.
[13] T. Sonoda, M. Kinoshita, N. Ishikawa, M. Sataka, A. Iwase, K. Yasunaga, Clarification of high density electronic excitation effects on the microstructural evolution in UO_2, Nucl. Instr. Meth. Phys. Res. B 268 (2010) 3277–3281.
[14] Hj. Matzke, P.G. Lucuta, T. Wiss, Swift heavy ion and fission damage effects in UO_2, Nucl. Instr. Meth. Phys. Res. B 166–167 (2000) 920–926.
[15] P.B. Weisensee, J.P. Feser, D.G. Cahill, Effect of ion irradiation on the thermal conductivity of UO_2 and U_3O_8 epitaxial layers, J. Nucl. Mater. 443 (2013) 212–217.
[16] N. Nakae, H. Akiyama, H. Miura, T. Baba, K. Kamimura, S. Kurematsu, Y. Kosaka, A. Yoshino, T. Kitagawa, Thermal property change of MOX and UO_2 irradiated up to high burnup of 74GWd/t, J. Nucl. Mater. 440 (2013) 515–523.
[17] J. Pakarinen, L. He, M. Gupta, J. Gan, A. Nelson, A. El-Azab, T.R. Allen, 2.6 MeV proton irradiation effects on the surface integrity of depleted UO_2, Nucl. Instr. Meth. Phys. Res. B 319 (2014) 100–106.
[18] V.G. Baranov, A.V. Lunev, A.V. Tenishev, A.V. Khlunov, Interaction of dislocations in UO_2 during high burn-up structure formation, J. Nucl. Mater. 444 (2014) 129–137.
[19] A.J. Popel, S. Le Solliec, G.I. Lampronti, J. Day, P.K. Petrov, I. Farnan, The effect of fission-energy Xe ion irradiation on the structural integrity and dissolution of the CeO_2 matrix, J. Nucl. Mater. 484 (2017) 332–338.
[20] H. Ohno, A. Iwase, D. Matsumura, Y. Nishihata, J. Mizuki, N. Ishikawa, Y. Baba, N. Hirao, T. Sonoda, M. Kinoshita, Study on effects of swift heavy ion irradiation in cerium dioxide using synchrotron radiation X-ray absorption spectroscopy, Nucl. Instr. Meth. Phys. Res. B 266 (2008) 3013–3017.
[21] A. Kumar, R. Devanathan, V. Shutthanandan, S.V.N.T. Kuchibhatla, A.S. Karakoti, Y. Yong, S. Thevuthasan, S. Seal, Radiation-induced reduction of ceria in single and polycrystalline thin films, J. Phys. Chem. C 116 (2012) 361–366.
[22] Yu.A. Teterin, A.S. Baev, Rentgenovskaya Fotoelektronnaya Spektroskopiya Soedinenii Lantanoidov (X-ray Photoelectron Spectroscopy of Lanthanide Compounds), TsNII atominform, Moscow, 1987 (in Russian).
[23] Yu.A. Teterin, A.Yu. Teterin, Structure of X-ray photoelectron spectra of lanthanide compound, Russ. Chem. Rev. 71 (2002) 347–381.
[24] A. Kotani, T. Jo, J.C. Parlebas, Many-body effects in core-level spectroscopy of rare-earth compounds, Adv. Phys. 37 (1988) 37–85.
[25] A. Kotani, H. Ogasawara, Theory of core-level spectroscopy of rare-earth oxides, J. Electron Spectrosc. Relat. Phenom. 60 (1992) 257–299.
[26] A. Kotani, Theory of core-level spectroscopy in *f* and *d* electron systems, J. Electron Spectrosc. Relat. Phenom. 100 (1999) 75–104.
[27] G. Praline, B.E. Koel, R.L. Hance, H.-I. Lee, J.M. White, X-ray photoelectron study of the reaction of oxygen with cerium, J. Electron Spectrosc. Relat. Phenom. 21 (1980) 17–30.
[28] B.E. Koel, G. Praline, H.-I. Lee, J.M. White, R.L. Hance, X-Ray photoelectron study of the reaction of water with cerium, J. Electron Spectrosc. Relat. Phenom. 21 (1980) 31–46.
[29] Yu.A. Teterin, T.N. Bondarenko, A.Yu. Teterin, A.M. Lebedev, I.O. Utkin, XPS of lanthanoide orthoniobates, J. Electron Spectrosc. Relat. Phenom. 96 (1998) 221–228.
[30] Yu.A. Teterin, A.Yu. Teterin, I.O. Utkin, M.V. Ryzhkov, XPS study of the Ln 5p,4f-electronic states of lanthanides in Ln_2O_3, J. Electron Spectrosc. Relat. Phenom. 137–140 (2004) 601–605.
[31] G. Kaindl, G.K. Wertheim, G. Schmiester, E.V. Sampathkumaran, Mixed valency versus covalency in rare-earth core-electron spectroscopy, Phys. Rev. Lett. 58 (1987) 606–609.
[32] E. Bêche, P. Charvin, D. Perarnau, S. Abanades, G. Flamant, Ce 3d XPS investigation of cerium oxides and mixed cerium oxide ($Ce_xTi_yO_z$), Surf. Interf. Anal. 40 (2008) 264–267.
[33] J.P. Holgado, R. Alvarez, G. Munuera, Study of CeO_2 XPS spectra by factor analysis: reduction of CeO_2, Appl. Surf. Sci. 161 (2000) 301–315.
[34] E. Paparazzo, XPS studies of damage induced by X-ray irradiation on CeO_2 surfaces, Surf. Sci. Lett. 234 (1990) L253–L258.
[35] Yu.A. Teterin, S.V. Stefanovskiĭ, S.V. Yudintsev, G.N. Bek-Uzarov, A.Yu. Teterin, K.I. Maslakov, I.O. Utkin, X-ray photoelectron study of calcium cerium titanate ceramics, Russ. J. Inorg. Chem. 49 (2004) 87–94.
[36] Yu.A. Teterin, A.Yu. Teterin, A.M. Lebedev, I.O. Utkin, X-ray photoelectron spectra of oxygen-containing cerium compounds, Radiochemistry 40 (1998) 101–106.
[37] P. Burroughs, A. Hamnett, A.F. Orchard, G. Thornton, Satellite structure in the *X*-ray photoelectron spectra of some binary and mixed oxides of lanthanum and cerium, J. Chem. Soc., Dalton Trans. (1976) 1686–1698.

[38] E. Paparazzo, G.M. Ingo, N. Zacchetti, X-ray induced reduction effects at CeO_2 surfaces: an x-ray photoelectron spectroscopy study, J. Vac. Sci. Technol. A 9 (1991) 1416–1420.
[39] A. Fujimori, Mixed-valent ground state of CeO_2, Phys. Rev. B 28 (1983) 2281–2283.
[40] E. Shoko, M.F. Smith, R.H. McKenzie, Mixed valency in cerium oxide crystallographic phases: valence of different cerium sites by the bond valence method, Phys. Rev. B 79 (2009) 134108.
[41] G. Thornton, M.J. Dempsey, Final-state effects in the 3d and 4d X-ray photoelectron spectra of CeO_2, Chem. Phys. Lett. 77 (1981) 409–412.
[42] Yu.A. Teterin, A.Yu. Teterin, A.M. Lebedev, I.O. Utkin, The XPS spectra of cerium compounds containing oxygen, J. Electron Spectrosc. Relat. Phenom. 88–91 (1998) 275–279.
[43] M.V. Ryzhkov, V.A. Gubanov, Yu.A. Teterin, A.S. Baev, Electronic structure, chemical bonding and X-ray photoelectron spectra of light rare-earth oxides, Z. Phys. B Con. Mat. 59 (1985) 1–6.
[44] F. Zhang, P. Wang, J. Koberstein, S. Khalid, S.-W. Chan, Cerium oxidation state in ceria nanoparticles studied with X-ray photoelectron spectroscopy and absorption near edge spectroscopy, Surf. Sci. 563 (2004) 74–82.
[45] E. Paparazzo, On the curve-fitting of XPS Ce(3d) spectra of cerium oxides, Mater. Res. Bull. 46 (2011) 323–326.
[46] B. Chen, Y. Ma, L. Ding, L. Xu, Z. Wu, Q. Yuan, W. Huang, Reactivity of hydroxyls and water on a CeO_2(111) thin film surface: the role of oxygen vacancy, J. Phys. Chem. C 117 (2013) 5800–5810.
[47] C.A. Strydom, H.J. Strydom, X-ray photoelectron spectroscopy determination of the Ce(III)/Ce(IV) ratio in cerium compounds, Inorg. Chim. Acta 161 (1989) 7–9.
[48] Yu.A. Teterin, A.J. Popel, K.I. Maslakov, A.Yu. Teterin, K.E. Ivanov, S.N. Kalmykov, R. Springell, T.B. Scott, I. Farnan, XPS Study of ion irradiated and unirradiated UO_2 thin films, Inorg. Chem. 55 (2016) 8059–8070.
[49] L.M. Liz-Marzán, Nanometals: formation and color, Mater. Today 7 (2004) 26–31.
[50] J.F. Ziegler, J.P. Biersack, M.D. Ziegler, The Stopping and Range of Ions in Matter, SRIM Co., Chester, Maryland, U.S.A., 2008.
[51] Yu.A. Teterin, A.Yu. Teterin, The structure of X-ray photoelectron spectra of light actinide compounds, Russ. Chem. Rev. 73 (2004) 541–580.
[52] D. Shirley, High-resolution X-ray photoemission spectrum of the valence bands of gold, Phys. Rev. B 5 (1972) 4709–4714.
[53] M. Engelhard, S. Azad, C.H.F. Peden, S. Thevuthasan, X-ray photoelectron spectroscopy studies of oxidized and reduced CeO_2(111) surfaces, Surf. Sci. Spec. 11 (2004) 73–81.
[54] L. Armelao, D. Barreca, G. Bottaro, A. Gasparotto, E. Tondello, Plasma-enhanced CVD CeO_2 nanocrystalline thin films analyzed by XPS, Surf. Sci. Spec. 8 (2001) 247–257.
[55] D.R. Mullins, S.H. Overbury, D.R. Huntley, Electron spectroscopy of single crystal and polycrystalline cerium oxide surfaces, Surf. Sci. 409 (1998) 307–319.
[56] M.V. Rama Rao, T. Shripathi, Photoelectron spectroscopic study of X-ray induced reduction of CeO_2, J. Electron Spectrosc. Relat. Phenom. 87 (1997) 121–126.
[57] V. Stetsovych, F. Pagliuca, F. Dvorak, T. Duchon, M. Vorokhta, M. Aulicka, J. Lachnitt, S. Schernich, I. Matolinova, K. Veltruska, T. Skala, D. Mazur, J. Myslivecek, J. Libuda, V. Matolin, Epitaxial cubic Ce_2O_3 films via Ce-CeO_2 interfacial reaction, J. Phys. Chem. Lett. 4 (2013) 866–871.
[58] Y. Zhu, N. Jain, M.K. Hudait, D. Maurya, R. Varghese, S. Priya, X-ray photoelectron spectroscopy analysis and band offset determination of CeO_2 deposited on epitaxial (100), (110), and (111)Ge, J. Vac. Sci. Technol. B 32 (2014) 011217.
[59] F. Le Normand, J. El Fallah, L. Hilaire, P. Légaré, A. Kotani, J.C. Parlebas, Photoemission on 3d core levels of Cerium: an experimental and theoretical investigation of the reduction of cerium dioxide, Solid State Commun. 71 (1989) 885–889.
[60] T. Hasegawa, S.M. Shahed, Y. Sainoo, A. Beniya, N. Isomura, Y. Watanabe, T. Komeda, Epitaxial growth of CeO_2(111) film on Ru(0001): scanning tunneling microscopy (STM) and X-ray photoemission spectroscopy (XPS) study, J. Chem. Phys. 140 (2014) 044711.
[61] I.M. Band, Y.I. Kharitonov, M.B. Trzhaskovskaya, Photoionization cross sections and photoelectron angular distributions for X-ray line energies in the range 0.132–4.509 keV targets: $1 \leq Z \leq 100$, Atom. Data Nucl. Data 23 (1979) 443–505.
[62] M.B. Trzhaskovskaya, V.G. Yarzhemsky, Dirac-Fock photoionization parameters for HAXPES applications, Atom. Data Nucl. Data 119 (2018) 99–174.
[63] A.Q. Wang, P. Punchaipetch, R.M. Wallace, T.D. Golden, X-ray photoelectron spectroscopy study of electrodeposited nanostructured CeO_2 films, J. Vac. Sci. Technol. B 21 (2003) 1169–1175.
[64] V.G. Yarzhemsky, Yu.A. Teterin, M.I. Sosulnikov, Dynamic dipolar relaxation in X-ray photoelectron spectra of the Ba4p subshell in barium compounds, J. Electron Spectrosc. Relat. Phenom. 59 (1992) 211–222.
[65] V.G. Yarzhemsky, Yu.A. Teterin, A.Yu. Teterin, M.Y. Amusia, V.I. Nefedov, Structure of X-ray photoelectron 4p-spectra of Xe and compounds of Cs, Ba, La, J. Synch. Investig. 6 (2005) 3–9 (in Russian).
[66] M.I. Sosulnikov, Yu.A. Teterin, X-ray photoelectron studies of Ca, Sr and Ba and their oxides and carbonates, J. Electron Spectrosc. Relat. Phenom. 59 (1992) 111–126.
[67] P.S. Bagus, C.J. Nelin, Y. Al-Salik, E.S. Ilton, H. Idriss, Multiplet splitting for the XPS of heavy elements: dependence on oxidation state, Surf. Sci. 643 (2016) 142–149.
[68] M. Wolcyrz, L. Kepinski, Rietveld refinement of the structure of CeOCI formed in Pd/CeO_2 catalyst: notes on the existence of a stabilized tetragonal phase of La_2O_3 in LaPdO system, J. Solid State Chem. 99 (1992) 409–413.
[69] A.J. Popel, T.W. Wietsma, M.H. Engelhard, A.S. Lea, O. Qafoku, C. Grygiel, I. Monnet, E.S. Ilton, M.E. Bowden, I. Farnan, The effect of ion irradiation on the dissolution of UO_2 and UO_2-based simulant fuel, J. Alloys Compd. 735 (2018) 1350–1356.